# Different Cerium Valence Transitions Observed by Hydrogenation of the Ternary Germanides CeRhGe and CeIrGe – Structure, Physical Properties and Chemical Bonding

Bernard Chevalier[a], Etienne Gaudin[a], Adel F. Al Alam[a], Samir F. Matar[a], François Weill[a,b], Birgit Heying[c], and Rainer Pöttgen[c]

[a] ICMCB, CNRS, Université Bordeaux 1, 87 Avenue du Docteur Albert Schweitzer, 33608 Pessac Cedex, France
[b] Centre de Ressource en Microscopie Electronique et Microanalyse, CREMEM, Université Bordeaux 1, Avenue des Facultés, Batiment B8, F-33400 Talence Cedex, France
[c] Institut für Anorganische und Analytische Chemie, Universität Münster, Corrensstraße 30, D-48149 Münster, Germany

Reprint requests to Dr. B. Chevalier. E-mail: chevalie@icmcb-bordeaux.cnrs.fr or Prof. Dr. R. Pöttgen. E-mail: pottgen@uni-muenster.de

*Z. Naturforsch.* **2008**, *63b,* 685 – 694; received January 15, 2008

*Dedicated to Professor Gérard Demazeau on the occasion of his 65$^{th}$ birthday*

The ternary germanides CeRhGe and CeIrGe which crystallize in the orthorhombic TiNiSi-type structure, absorb hydrogen at 523 K. X-Ray powder diffraction and transmission electron microscopy indicate that the hydrides $CeRhGeH_{1.8}$ and $CeIrGeH_{1.8}$ adopt the hexagonal ZrBeSi-type structure. Magnetization, electrical resistivity and thermoelectric power measurements reveal that these hydrides are intermediate-valence compounds. An unusual transition from antiferromagnetic to spin fluctuation behavior occurs upon hydrogenation of CeRhGe, while on the contrary, $CeIrGeH_{1.8}$ presents a Kondo temperature of 285 K smaller than that observed for CeIrGe (610 K). In order to explain these opposite valence transitions, the electronic structures of the hydrides have been self-consistently calculated within the local spin density functional theory (LSDF). The structures are compared to those reported previously by us for CeRhGe and CeIrGe.

*Key words:* Hydrogenation, Structural Transition, Intermediate-valence Compounds, Electronic Structure Calculation

## Introduction

The equiatomic ternary germanides CeRhGe and CeIrGe crystallize as isopointal variants of the well known orthorhombic TiNiSi-type structure. Both compounds have been intensively investigated in recent years with respect to their peculiar magnetic and electrical properties. An overview on the relevant literature is given in references [1, 2]. Due to different tilts within the polyanionic [RhGe] and [IrGe] networks, CeRhGe and CeIrGe exhibit differences in the Ce–Rh and Ce–Ir bonding, respectively, leading to different magnetic behavior, *i. e.* CeRhGe orders antiferromagnetically at $T_N$ = 9.3 K with an incommensurate magnetic structure, while CeIrGe is an intermediate-valence system [3 – 6].

CeRhGe shows a structural [7] and magnetic phase transition [6] near 510 K. This first-order transition is accompanied by a significant hysteresis. Similar behavior can be induced by partly substituting rhodium by iridium. A sample of composition $Ce(Rh_{0.69}Ir_{0.31})Ge$ shows a first-order valence transition of cerium in the temperature range 236 – 258 K [1] with essentially trivalent cerium below 200 K and an intermediate-valent cerium above 300 K. This transition constitutes the first example of this kind among cerium intermetallics; the valence of cerium increases with temperature.

Modification of the physical properties of such intermetallic cerium compounds is possible through the application of high pressure or *via* hydrogenation. In the latter case hydrogen acts as a kind of 'negative' pressure. To give two recent examples, hydrogenation of CeRhSb, and the solid solution $Ce(Rh_{1-x}Ir_x)Ga$ lead to an antiferromagnetic behavior in the hydrides $CeRhSbH_{0.2}$ [8] and $Ce(Rh_{1-x}Ir_x)GaH_{1.8}$ [9].

Overviews on the structure-property relationships of various hydrides of Ce*TX* (*T* = late transition metal; *X* = element of the 3rd and 4th main group) intermetallics are given in [10] and [11].

In view of the interesting properties of CeRhGe and CeIrGe, we have also tested the hydrogenation behavior of these germanides. Herein we give a detailed report on the structure, physical properties and chemical bonding of the hydrides $CeRhGeH_{1.8}$ and $CeIrGeH_{1.8}$.

## Experimental Section

*Synthesis*

Starting materials for the preparation of CeRhGe and CeIrGe were sublimed ingots of cerium (Johnson Matthey), rhodium and iridium powders (Degussa-Hüls, 200 mesh), and germanium lumps (Wacker), all with stated purities better than 99.9 %. CeRhGe and CeIrGe were prepared *via* arc-melting [12] of the elements. For both syntheses, the cerium pieces were first arc-melted to small buttons of about 500 mg. The argon was purified over titanium sponge (900 K), silica gel, and molecular sieves. The pre-melting procedure strongly reduces shattering during the subsequent reactions with rhodium, iridium and germanium. The cerium buttons were then mixed with the rhodium or iridium powder (cold-pressed to pellets of 6 mm diameter) and pieces of the germanium lumps. The mixtures of the three elements were then reacted and remelted three times to ensure homogeneity. The total weight losses after the melting procedures were always smaller than 0.5 %. The resulting polycrystalline samples were light gray with metallic luster. They are stable in moist air.

The purity of the CeRhGe and CeIrGe samples was checked through Guinier powder patterns using Cu$K_{\alpha 1}$ radiation and $\alpha$-quartz ($a$ = 491.30, $c$ = 540.46 pm) as an internal standard. The Guinier camera was operated with an image plate system (Fujifilm, BAS-1800). The experimental patterns were compared with calculated ones [13] taking the atomic positions from the structure refinements [1]. In X-ray powder diffraction studies no parasitic phase was detected, confirming that these ternary germanides crystallize in the orthorhombic TiNiSi-type structure with unit cell parameters in agreement with those reported previously [3].

*Hydrogenation experiments*

Hydrogen absorption experiments were performed using the apparatus described previously [14]. An annealed ingot of CeRhGe or CeIrGe was heated under vacuum at 523 K for 12 h and then exposed for two days to 4 MPa of hydrogen gas at the same temperature. The amount of inserted H was determined volumetrically by monitoring pressure changes in a calibrated volume. Under the experimental conditions described above, the ternary germanides absorb hydrogen. The molar amount of hydrogen inserted is 1.8(1) per CeRhGe or CeIrGe formula unit. The hydrides formed are stable in air and show a metallic aspect. Also, the H-absorption induces a decrepitation of the pure starting ingot into small grains.

X-Ray powder diffraction with the use of a Philips 1050-diffractometer (Cu$K_\alpha$ radiation) was applied for the characterization of the structural type and for the phase identification of the hydrides. The unit cell parameters were determined by a least-squares refinement method using silicon (5N) as an internal standard.

*Transmission electron microscopy*

The electron diffraction investigation was carried out on a JEOL 2000FX microscope, operating at 200 kV, equipped with a double tilt specimen stage. Prior to the investigation, the hydrides were crushed in an agate mortar under alcohol. A drop of the suspension was deposited on a carbon-supported grid.

*Physical property measurements*

For transport measurements, the hydrides $CeRhGeH_{1.8}$ and $CeIrGeH_{1.8}$ were compacted at r. t. (compactness $\cong$ 80 %) in order to form a polycrystalline pellet (diameter = 6 mm and thickness = 3 mm) and then heated for one week at 523 K under a pressure (4 MPa) of hydrogen. After this thermal treatment, which improved the mechanical behavior, the pellet was checked by X-ray diffraction; no structural change was evident. Thermoelectric power measurements were performed on this pellet using a dynamic method. Details of the cell used and of the measurement methods were described previously [15]. For electrical resistivity measurements, a bar of $1.5 \times 1.5 \times 5$ mm$^3$ was cut from the pellet. The measurement was carried out above 4.2 K using the standard dc four probe method with silver paint contacts and an intensity current of 10 mA. *Due to the presence of microcracks in the samples, the absolute value of* $\rho$ *could not be determined accurately; for this reason, a reduced representation* $\rho/\rho$ *(270 K) is chosen*. Finally, magnetization measurements were performed on a part of the pellet using a Superconducting Quantum Interference Device (SQUID) magnetometer in the temperature range 1.8 – 350 K and applied fields up to 4.6 T. Similar measurements were performed on the initial ternary germanides. In order to compare the electrical resistivity and the thermoelectric power of CeRhGe, CeIrGe and their hydrides, we have used similar bars (same size) and similar contact positions. These conditions minimize the differences between the geometrical factors.

*Computational details*

The electronic structure calculations were performed within the density functional theory (DFT) [16, 17] making

use of the all-electron scalar relativistic augmented spherical wave (ASW) method [18 – 20]. A local spin density approximation (LSDA) was used for an account of the effects of exchange and correlation following the scheme of Vosko *et al.* [21]. All valence states, including the $4f$(Ce) orbitals, were treated as band states. In the minimal ASW basis set, the outermost shells were chosen to represent the valence states using partial waves up to $l_{max} + 1 = 4$ for Ce, $l_{max} + 1 = 3$ for Rh and Ge, and $l_{max} + 1 = 2$ for H. For germanium, the $3d^{10}$ states were considered as core states, thus allowing for empty $4d^0$ states to be part of the trial basis set. The ASW method is equally based on the atomic sphere approximation (ASA) which optimizes atomic sphere radii, thus ensuring for minimal overlap within these spheres. In order to establish $l$-expansion convergence, *i. e.* avoiding an otherwise too large overlap between the actual atomic spheres, additional augmentation spheres, called empty spheres (ES: "pseudo atoms" with zero atomic numbers), were introduced to represent the interstitial space without loss of crystal symmetry. This was especially applied for the hydride "$CeRhGeH_2$" due to its less compact structure as compared to the ternary germanide CeRhGe. ESs receive charges from neighboring atomic species. The self-consistent field calculations were run until a convergence of the total energy ($\Delta E = 10^{-8}$ Ryd) and of the charges ($\Delta Q = 10^{-8}$) between two subsequent iterations was reached. For that a progressive increase of the Brillouin zone (BZ) integration up to a value of 576 k points, *i. e.* 16 k points in each direction of the irreducible wedge of the hexagonal BZ, was used. The crystal structure determined for the hydride based on rhodium was used for the computation of the electronic structure. A non-spin polarized (NSP) configuration, meaning that the spin degeneracy is enforced for all atoms, was assumed to assess the chemical bonding properties. Information about the nature of the interactions between the atomic constituents is obtained here using the so-called ECOV (covalent bond energy) criterion [22] which is a slight refinement combining both overlap and Hamiltonian based criteria, COOP [23] and COHP [24], to calculate quantities independent of the choice of the potential zero.

## Results and Discussion

### *Structural properties*

The examination of some small crystals of $CeRhGeH_{1.8}$ and $CeIrGeH_{1.8}$ by transmission electron microscopy reveals that the absorption of hydrogen by the initial ternary germanides modifies their structural properties. As an example, for $CeRhGeH_{1.8}$, selected-area electron diffraction patterns along the zone axis [001], [010] and [$\bar{1}$10] are shown in Fig. 1. This study indicates a hexagonal symmetry of the crystal structure of the hydride (see the characteristic pattern along the [001] direction). Further, the pattern along the [$\bar{1}$10] zone axis indicates a reflection condition $hhl$ with $l = 2n$. This agrees with the presence of a $c$-type glide plane as for the hexagonal ZrBeSi-type structure (space group $P6_3/mmc$). This result is confirmed by X-ray powder diffraction performed on the hydrides (Fig. 2). The patterns can be totally indexed on the basis of a hexagonal unit cell with the ZrBeSi-type structure. The unit cell parameters deduced from this analysis are $a$ = 429.4 and $c$ = 855.8 pm for $CeRhGeH_{1.8}$ and $a$ = 434.4 and $c$ = 847.9 pm for $CeIrGeH_{1.8}$. In the sequence $CeRhGeH_{1.8} \rightarrow CeIrGeH_{1.8}$, the $a$ parameter increases whereas the $c$ parameter decreases. This is evidenced by the examination of the patterns presented in Fig. 2; for the hydride $CeRhGeH_{1.8}$ the two peaks 110 and 004 appear practically at the same $2\theta$ angle, but on the contrary in $CeIrGeH_{1.8}$ the 110 peak is observed at a smaller $2\theta$ angle whereas the 004 peak is detected at a higher $2\theta$ angle (inset of Fig. 2). This observation agrees with the evolution of the $a$ and $c$ parameter in the sequence $CeRhGeH_{1.8} \rightarrow CeIrGeH_{1.8}$. Similar behavior reported recently during the hydrogenation of the $Ce(Rh_{1-x}Ir_x)Ga$ system [9] was explained as follows: (i) the hexagonal ZrBeSi-type of the hydrides can be described as planes perpendicular to the $c$ axis with the sequence (Rh or Ir, Ga or Ge)–Ce–(Rh or Ir, Ga or Ge)–Ce (Fig. 3); (ii) the presence of a 2D (Rh or Ir, Ga or Ge)-substructure perpendicular to the

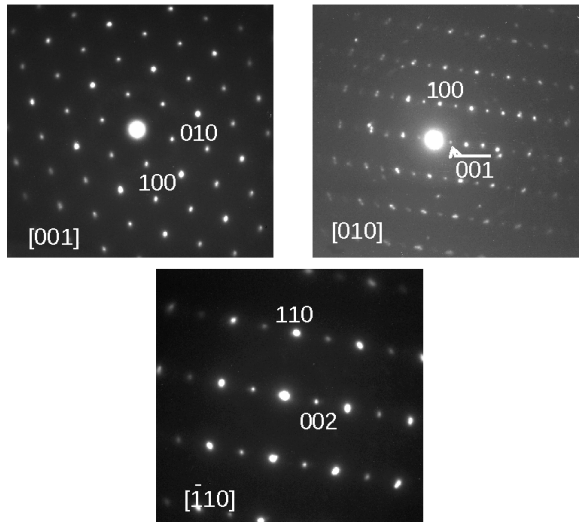


Fig. 1. Electron diffraction patterns of the hydride $CeRhGeH_{1.8}$ along the [001], [010] [$\bar{1}$10] directions.

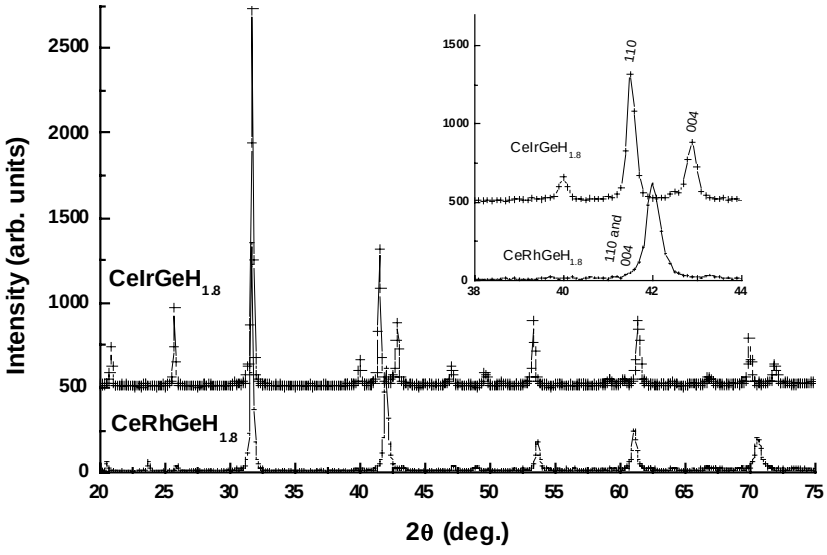


Fig. 2. X-Ray powder diffraction patterns of the hydrides $CeRhGeH_{1.8}$ and $CeIrGeH_{1.8}$. Inset: for $38 \leq 2\theta \leq 44°$ the Miller indices 110 and 004 are given.

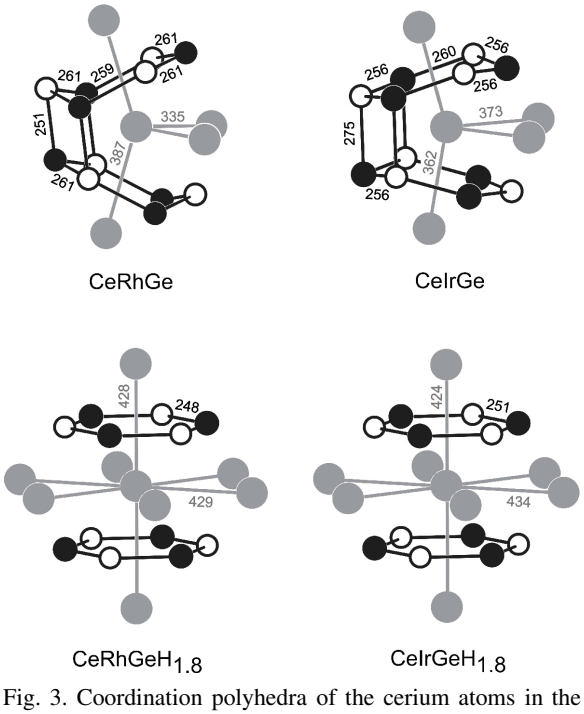


Fig. 3. Coordination polyhedra of the cerium atoms in the ternary germanides CeRhGe and CeIrGe and the corresponding hydrides. The cerium, transition metal ($T$), and germanium atoms are drawn as medium gray, black filled, and open circles, respectively. Relevant interatomic distances are given in units of pm. The hydrogen sites (not determined) are not shown.

$c$ axis influences the $a$ parameter; as Ir is bigger than Rh this parameter increases; (iii) consequently, in order to keep similar Ce–Rh/Ir and Ce–Ge distances in the hydrides, the $c$ parameter decreases. In $CeRhGeH_{1.8}$ and $CeIrGeH_{1.8}$, the distances Ce–Rh = 327.5 pm and Ce–Ir = 328.4 pm agree with the increase of the covalent radii in the sequence Rh (125 pm) → Ir (126 pm).

Finally, the structural transition from the orthorhombic TiNiSi type to the hexagonal ZrBeSi type observed during the hydrogenation of CeRhGe and CeIrGe is similar to that previously observed by hydrogen insertion into CeNiGe [25], CeNiSn [26], CeRhGa and CeIrGa [9]. This transition induces an increase of the molar volume $V_m$ which is 15.6 and 18.3 % for the hydrogenation of CeRhGe and CeIrGe, respectively. We note that $V_m = 0.0591$ nm$^3$ for CeRhGe is higher than $V_m = 0.0586$ nm$^3$ for CeIrGe [1] whereas $V_m = 0.0683$ nm$^3$ for $CeRhGeH_{1.8}$ is smaller than $V_m = 0.0692$ nm$^3$ for $CeIrGeH_{1.8}$. These steric considerations suggest (i) a strong modification of the strength of $4f$(Ce)-ligand interactions responsible for the electronic state of cerium in these ternary germanides, and (ii) a different influence of the hydrogenation on their physical properties since during the hydrogen insertion the volumes $V_m$ change differently.

*Magnetic, electric and thermoelectric properties*

In Fig. 4 the temperature dependence of the reciprocal magnetic susceptibility $\chi_m^{-1}$ of CeRhGe and its hydride is compared. Above 100 K, the $\chi_m^{-1} = f(T)$ curve for CeRhGe follows a Curie-Weiss law with the effective magnetic moment $\mu_{eff} = 2.23\ \mu_B$/Ce and the

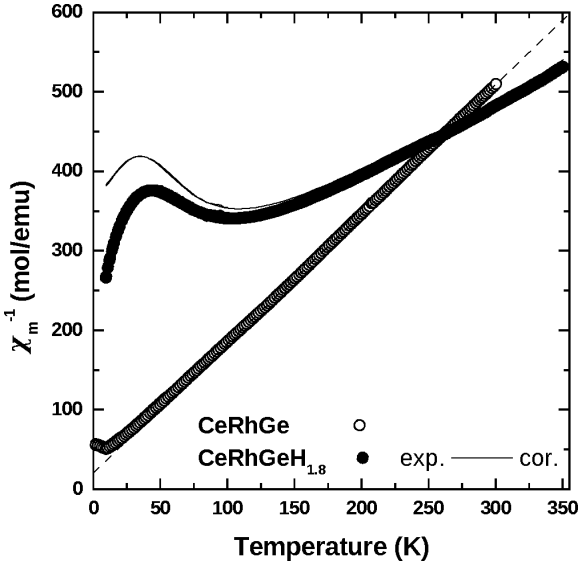


Fig. 4. Temperature dependence of the reciprocal magnetic susceptibility ${\chi_\mathrm{m}}^{-1}$, measured with an applied field of 4 T, for the ternary germanide CeRhGe and its hydride. The dashed line represents the Curie-Weiss law and the solid line the reciprocal corrected susceptibility $[\chi_\mathrm{m} - nC/T]^{-1}$ (see text).

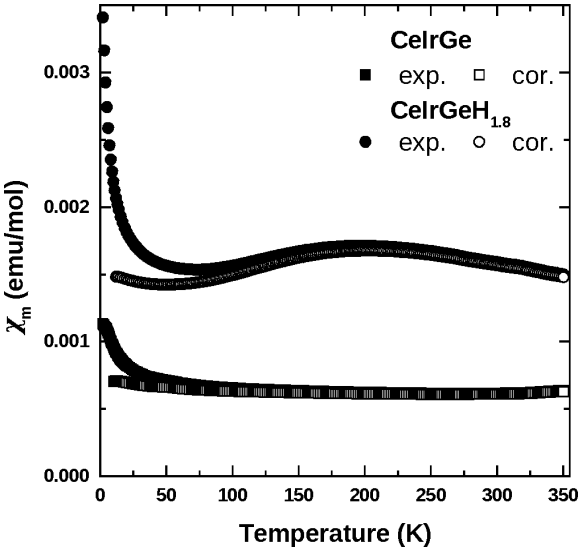


Fig. 5. Temperature dependence of the magnetic susceptibility $\chi_\mathrm{m}$, measured with an applied field of 4 T, for the ternary germanide CeIrGe and its hydride. The open symbols show the corrected susceptibility $[\chi_\mathrm{m} - nC/T]$ (see text).

paramagnetic Curie temperature $\theta_\mathrm{p} = -13$ K. These values are close to those reported previously [3]; the $\mu_\mathrm{eff}$ value agrees with a trivalent state for Ce. The presence of a minimum around 9 – 10 K confirms the antiferromagnetic ordering of CeRhGe [3]. The curve ${\chi_\mathrm{m}}^{-1} = f(T)$ for CeRhGeH$_{1.8}$ shows a different behavior: (i) there is no evidence for Curie-Weiss dependence; (ii) the presence of a broad minimum around 90 – 110 K is a characteristic of valence fluctuating systems [27] and (iii) the decrease of ${\chi_\mathrm{m}}^{-1}$ below 35 – 45 K appears to originate from a small amount of free $Ce^{3+}$ ions stabilized owing to lattice defects as often observed in other valence-fluctuating systems [28]. According to this scheme, $\chi_\mathrm{m}$ of the hydride CeRhGeH$_{1.8}$ can be expressed at low temperatures ($< 45$ K) by $\chi_\mathrm{m} = \chi_\mathrm{m}(0) + nC/T$ where $\chi_\mathrm{m}(0)$ is the magnetic susceptibility at $T = 0$ K, $n$ is the proportion of stable $Ce^{3+}$ moments related to the trace of magnetic impurities, and $C = 0.807$ emu K mol$^{-1}$ is the Curie constant for free $Ce^{3+}$ ions. The best agreement between experimental and calculated $\chi_\mathrm{m}$ values leads to $\chi_\mathrm{m}(0) = 2.43 \times 10^{-3}$ emu mol$^{-1}$ and $n = 13.4 \times 10^{-3}$ $Ce^{3+}$ ions mol$^{-1}$. Fig. 4 presents the corrected function $[\chi_\mathrm{m} - nC/T]^{-1} = f(T)$ for reciprocal magnetic susceptibility *versus* temperature resulting from this calculation. This curve goes through a large minimum near 95 K; this temperature is almost fully consistent with the model offered by Lawrence *et al.* [27] which predicts that the temperature dependence of the corrected reciprocal susceptibility exhibits a minimum at $T = T_\mathrm{sf}/2$ where $T_\mathrm{sf} = C/2\chi_\mathrm{m}(0) = 166$ K is the spin fluctuation temperature resulting from the hybridization between $4f$(Ce) and conduction electrons. This analysis suggests that the hydrogenation of CeRhGe leads to a behavior corresponding to an antiferromagnet → spin fluctuation transition.

An appreciable increase in the $\chi_\mathrm{m}$ value of the hydride CeIrGeH$_{1.8}$ is observed relative to that of CeIrGe (Fig. 5). Above 50 K, $\chi_\mathrm{m}$ of CeIrGe decreases up to 250 K, and then increases slowly with temperature (the upturn below 50 K is attributed to the presence of traces of a magnetic impurity). This behavior characterizes a nearly Pauli paramagnet indicating that the $4f$(Ce) electrons are strongly hybridized with those of the conduction band [29, 30]. Using the model described by Lawrence *et al.* [27], we estimate a $T_\mathrm{sf}$ of 610 K. The curve $\chi_\mathrm{m} = f(T)$ concerning the hydride CeIrGeH$_{1.8}$ shows a broad maximum centered around 180 – 200 K, characteristic of an intermediate-valence system [27]. The analysis of these data as reported above gives $\chi_\mathrm{m}(0) = 1.49 \times 10^{-3}$ emu mol$^{-1}$, $n = 8.7 \times 10^{-3}$ $Ce^{3+}$ ions mol$^{-1}$ and $T_\mathrm{sf} = 285$ K, a

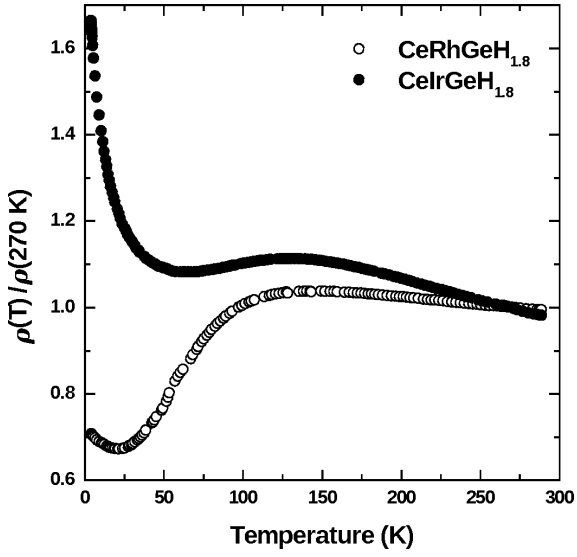


Fig. 6. Temperature dependence of the reduced electrical resistivity for the hydrides $CeRhGeH_{1.8}$ and $CeIrGeH_{1.8}$.

spin fluctuation temperature higher than that observed for $CeRhGeH_{1.8}$ ($T_{sf}$ = 166 K). From this $T_{sf}$ = 285 K value, it is expected that the $\chi_m = f(T)$ curve possesses a broad maximum near $T_{sf}/2$ = 142 K which is comparable with the experimental value of 180 – 200 K. It can be concluded that the hydrogen insertion into CeIrGe induces a decrease of the mixing between the states of the $4f$(Ce) and of the conduction electrons, but the resulting hydride may be considered as a valence-fluctuating compound. A similar result was reported for the product of the hydrogenation of the ternary germanide CeNiGe [25].

The temperature dependence of the reduced electrical resistivity of $CeRhGeH_{1.8}$ and $CeIrGeH_{1.8}$ exhibits some characteristics of Kondo systems (Fig. 6). Starting from 290 K, $\rho$ for $CeRhGeH_{1.8}$ first increases slightly with decreasing temperature, then goes through a broad maximum around 145 K, and then exhibits a minimum at about 45 K followed by a small increase down to 4.2 K. The variation above 45 K is very similar to that observed in many intermediate-valence systems [30, 31]. It is noted that the temperature (145 K) at which $\rho$ goes through a maximum is close (166 K) to that of the minimum in $\chi_m{}^{-1} = f(T)$ (Fig. 4). This agrees with the interpretation that the resistivity peak is due to a spin-scattering mechanism in the intermediate-valence regime [32]. Finally, the increase observed below 45 K could be explained by the Kondo effect on the magnetic impurity detected by magnetization measurements. The curve $\rho = f(T)$ concerning the other intermediate-valence hydride $CeIrGeH_{1.8}$ presents the same characteristics: a broad maximum near 150 K and a pronounced increase below 50 K.

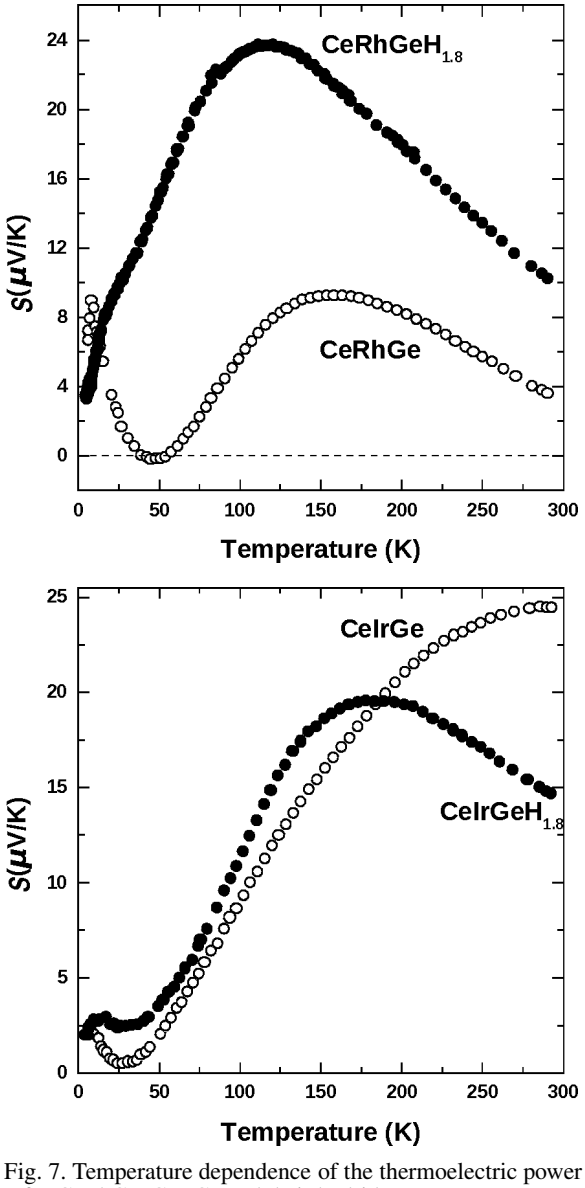


Fig. 7. Temperature dependence of the thermoelectric power $S$ for CeRhGe, CeIrGe and their hydrides.

Fig. 7 compares the temperature dependence of the thermopower of CeRhGe, CeIrGe and their hydrides. No data concerning the ternary germanides are available in the literature. The curve $S = f(T)$ for CeRhGe is mainly characterized by the exis-

tence of three extremes: a positive maximum of about 9 $\mu$V K$^{-1}$ near 155 K, a slightly negative value of $-0.5$ $\mu$V K$^{-1}$ around 45 K and a pronounced positive value of 9 $\mu$V K$^{-1}$ at 9 K associated with the occurrence of antiferromagnetic ordering. There is also a change in sign at 55 K. A similar change in sign has been observed for nearly trivalent cerium-based compounds such as $CeCu_2Si_2$, $CeAl_2$ and $CeAl_3$ [32]. In other words, the $S = f(T)$ curve for CeRhGe, which is comparable to that reported for CePdGe [25], agrees with the trivalent state of cerium in this ternary germanide.

The behavior of the other $S = f(T)$ curves observed for CeIrGe and the two hydrides are different. At r. t., CeIrGe presents a much larger thermopower (24 $\mu$V K$^{-1}$) than a normal metal. This behavior, observed also for CeNiGe [28, 34], is connected with the intermediate-valence state of cerium in this compound (very high Kondo temperature). Below 300 K, $S$ for CeIrGe is always positive implying that the dominant carriers are holes. Between 300 and 30 K, $S$ decreases from 24 to 1 $\mu$V K$^{-1}$, then increases and exhibits a maximum around 10 K. The $S = f(T)$ curve of CeIrGe resembles that observed for $CePd_3$ which is well known as a canonical intermediate-valence compound [33, 35]. $S$ for the hydride $CeIrGeH_{1.8}$ is mainly characterized by the existence of two positive maxima: one of about 20 $\mu$V K$^{-1}$ near 175 K and the second more narrow one at 3 $\mu$V K$^{-1}$ around 15 K, followed by a decrease. Between them, $S$ passes through a broad minimum close to 35 K. This behavior can be qualitatively understood in terms of the Coqblin–Schrieffer model (CSM) which ascribes the dynamics of conduction electrons to the exchange and potential scattering on incoherent $4f$(Ce) states [36, 37]. This model uses the crystalline electric field (CEF) ($\Delta$ as energy separation between ground and excited levels) and the number of $4f$(Ce) electrons ($n_f \leq 1$ for cerium). The curve $S = f(T)$ for $CeIrGeH_{1.8}$ is obtained for the CSM model with large CEF splitting and $n_f < 1$ (strong Kondo temperature $T_K$ as in intermediate-valence compounds). This assumption agrees with the existence of a large maximum around 150 K for the temperature dependence of the electrical resistivity of $CeIrGeH_{1.8}$ (Fig. 6); this behaviour is due to a spin scattering mechanism in the intermediate-valence regime [38].

Finally, $S$ for $CeRhGeH_{1.8}$ is always positive, presenting a maximum (24 $\mu$V K$^{-1}$) near 120 K and a shoulder around 20–30 K. These data resemble those reported for the intermediate-valence compound CeNiGe [28, 34] and confirm that the hydrogenation of CeRhGe induces a valence transition for cerium from a trivalent state to an intermediate-valence state. The two curves $S = f(T)$ observed for CeRhGe and its hydride, can be compared to those described recently by Link *et al.* [39], who have applied isostatic pressure on the ternary silicide $CePd_2Si_2$. Without pressure, $S$ of this compound exhibits at low temperature a negative peak followed by a broad positive contribution with increasing temperature. On the contrary, under a pressure of 5.6 GPa the curve $S = f(T)$ is always positive showing a shoulder at low temperature and a clear peak at high temperature. The transition between these two behaviors is explained by the sequence nearly trivalent cerium → intermediate-valent cerium induced by pressure. A similar sequence has been detected here by insertion of H atoms into CeRhGe. This result shows that this hydrogenation can be considered equivalent to an application of pressure on the ternary germanide.

*Density of states and chemical bonding*

*Projected Density of States – PDOS*

The site projected DOS, accounting for site multiplicity within the hexagonal structure of CeRhGe $H_2$ (the calculation was performed on the basis of a full occupation of the sites devoted for hydrogen), is given in Fig. 8; for the sake of clear presentation, the H partial PDOS are multiplied by 5. In this panel as well as in following ones, the zero energy is at the Fermi level ($E_F$). Just like in the pristine ternary germanide systems [2], the cerium PDOS are seen to prevail through a large peak around $E_F$ mainly due to $4f$(Ce) states which show larger localization (sharper and narrower peaks) around $E_F$. The computations for both CeRhGe and the hydride $CeRhGeH_2$ give DOS values for $4f$(Ce) states at $E_F$ levels such as 3.047 and 2.242 eV$^{-1}$, respectively. Subsequently, the cerium PDOS peak near $E_F$ is weaker in intensity for the hydride with respect to the pristine ternary germanide. The transition metal $4d$(Rh) states are found in the energy range from $-5$ to $-1$ eV with very small contributions to $E_F$. Their centering at a low energy of $-3$ eV is the result of the filling of the $4d$(Rh) states with 7 electrons. The larger broadening of $4d$ states is further enhanced by the mixing with the valence states of neighboring atoms. Theoretical calculations have presented a ($E$–$E_F$) value of $-1.613$ eV, higher than

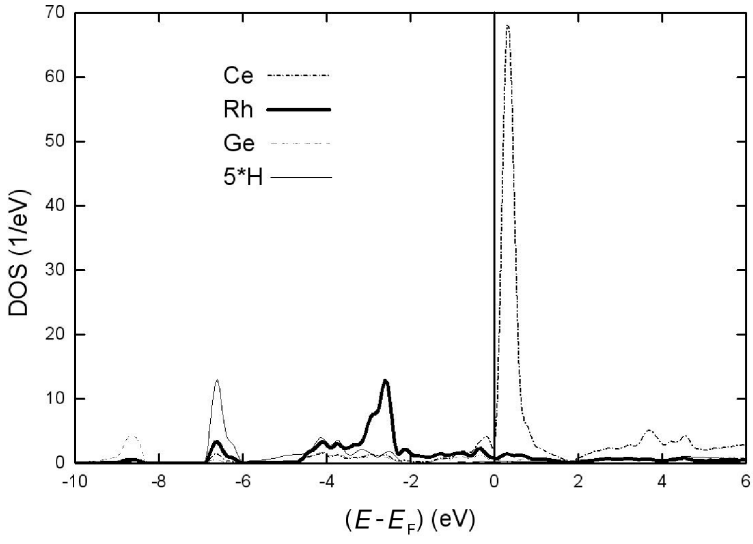


Fig. 8. Site projected partial DOS (PDOS) within $CeRhGeH_2$. The H PDOS is artificially multiplied by 5 for sake of presentation.

the computed value of −2.044 eV for CeRhGe. This is pertinent to the greater value for the Hankel energy of 7.783 eV determined for the hydride with respect to the value of 6.842 eV for the ternary germanide, thus confirming the hybridization between 4*d*(Rh) states and the valence states of other atoms. Around −7 eV, the itinerant Ce, Rh and H PDOS show similar skylines which are an indication of quantum mixing between these atomic species. These peaks owe their presence to hydrogen because they are not found in the DOS plot for CeRhGe [2]. It becomes relevant to discuss the changes of the interatomic distances within the metal substructure upon hydrogenating the CeRhGe system, which are $d_{Rh-Ge}$ = 258/248 pm and $d_{Ce-Rh}$ = 305/328 pm. These changes of magnitudes should have consequences on the chemical bonding the features of which are addressed in the next paragraph.

*Chemical bonding from the ECOV criterion*

The chemical bonding properties are analyzed here with the covalent bond energy ECOV criterion. In the unit-less plots, negative, zero and positive ECOV magnitudes (along the *y* axis) point to bonding, non-bonding and anti-bonding interactions respectively. Figs. 9(a) and (b) provide the ECOV for the atom-to-atom interactions within $CeRhGeH_2$ for the metal substructure and for the metal-hydrogen bonding, respectively. In Fig. 9(a), the major interaction is found between Rh and Ge which is of a bonding character between −5 and −2 eV in the VB. This follows from the reduction of $d_{Rh-Ge}$ from 258 to 248 pm upon hydrogenation. However, the largely bonding contribution around −4 eV is compensated by the anti-bonding peaks around the Fermi level. The second type of interactions arises for Ce–Rh with similar trends regarding the bond character as that shown for Rh–Ge throughout the VB up to $E_F$. Moreover, the Rh–Ge and Ce–Rh interactions are largely anti-bonding above $E_F$. Furthermore, a little contribution can be seen for the Ce–Ge bonding; contrary to former types of bond, these interactions are bonding throughout the VB and above $E_F$, so that their contribution stabilizes the system. A former study for the CeRhGe system (inset of Fig. 9(a)) [2] showed that the strongest bonding interaction throughout the VB is Ce–Rh followed by Ce–Ge, while above $E_F$ the interactions are found to be largely anti-bonding with the main contribution arising from Ce–Rh and Ce–Ge. In order to compare these results with the computed results for the hydride, the inner panel in Fig. 9(a), which represents the ECOV interactions plotted considering the 4*f*(Ce) states, is addressed. It can be seen that the atom-to-atom interactions have the same tendencies, while they are of a stronger character within $CeRhGeH_2$.

The analysis of the chemical bonding of hydrogen with the different atomic species is shown in Fig. 9(b). The Rh–H as well as Ce–H interactions are dominant throughout the VB and up to $E_F$. This is concomitant with the Ce–H and Rh–H bond lengths which are 254 and 160 pm, respectively. While the Rh–H bond should be favored with respect to the Ce–H bond, the

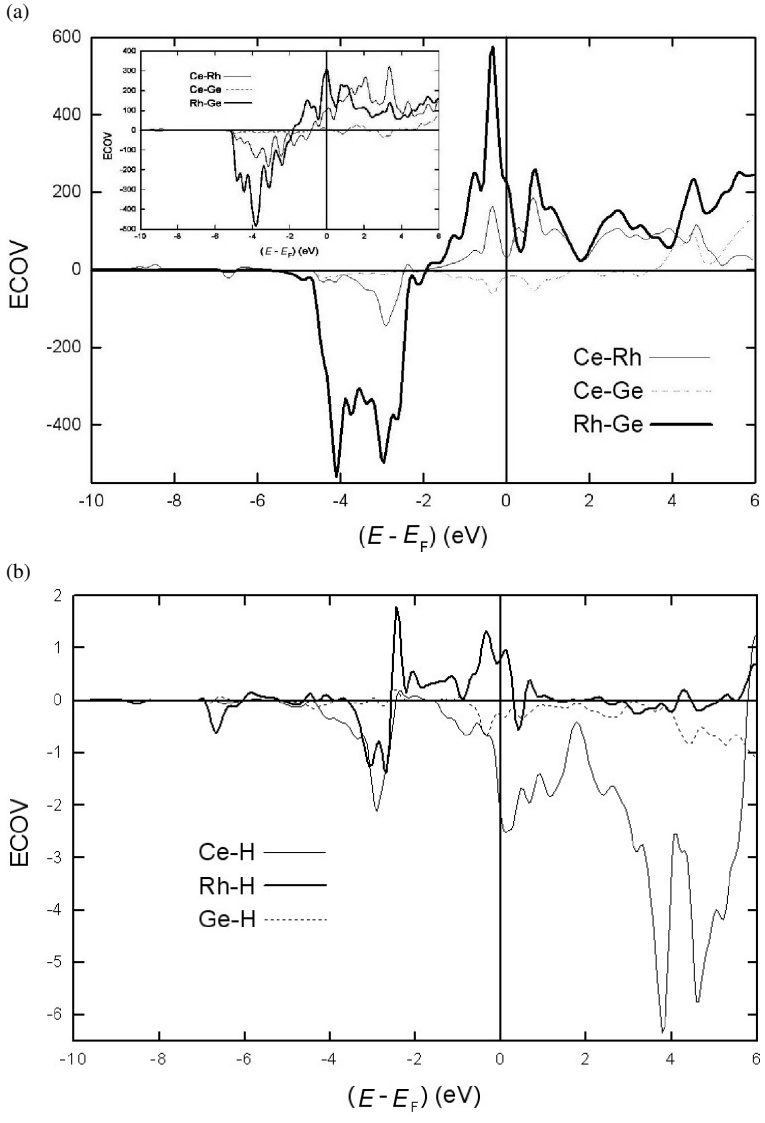


Fig. 9. Chemical bonding for atom-to-atom interactions within $CeRhGeH_2$: (a) the metal substructure (inset for CeRhGe [2]) and (b) the metal-H substructure.

similar magnitudes of the ECOV are partly due to the change of the structure from orthorhombic to hexagonal, whereby there is a reinforcement of the Rh–Ge interaction within the hydride, thus leaving less states for Rh to engage with H.

## Conclusion

Hydrogenation of the ternary germanides CeRhGe and CeIrGe has been reported for the first time. The hydrogen insertion into these compounds induces a structural transition from the orthorhombic TiNiSi to the hexagonal ZrBeSi type. The hydrogenation modifies also the valence states of cerium: a transition from an antiferromagnetic to an intermediate-valence compound is evidenced by magnetization, electrical resistivity and thermoelectric power measurements, for the sequence CeRhGe $\rightarrow$ $CeRhGeH_{1.8}$, whereas the influence of the Kondo effect is decreased by H insertion into CeIrGe. The magnetic transition observed for the rhodium-based compounds results from the Ce–Rh interactions; below $E_F$, this interaction is bonding in CeRhGe, but anti-bonding around $E_F$ in the hydride $CeRhGeH_{1.8}$. On the other hand, theoretical calculations provided an explanation for the valence behavior of Ce upon hydrogenation, relevant to the bonding character of the Ce – H interaction.

*Acknowledgements*

The authors would like to thank R. Decourt for his assistance during the electrical resistivity and thermoelectric power measurements. This work was financially supported by the Deutsche Forschungsgemeinschaft. B. C., E. G. and R. P. are indebted to EGIDE and DAAD for research grants within the PROCOPE program (11457RD and D/0502176). Finally, B. C. thanks the European Science Foundation (ECOMCOST action P16) for financial support.

[1] E. Gaudin, B. Chevalier, B. Heying, U. Ch. Rodewald, R. Pöttgen, *Chem. Mater*. **2005**, *17*, 2693.
[2] S. F. Matar, E. Gaudin, B. Chevalier, R. Pöttgen, *Solid State Sci*. **2007**, *9*, 274.
[3] P. Rogl, B. Chevalier, M. J. Besnus, J. Etourneau, *J. Magn. Magn. Mater*. **1989**, *80*, 305.
[4] B. Chevalier, P. Rogl, J. Etourneau, M. J. Besnus, *J. Magn. Magn. Mater*. **1990**, *83*, 303.
[5] B. Chevalier, P. Rogl, E. K. Hlil, M. H. Tuilier, P. Dordor, J. Etourneau, *Z. Phys. B* **1991**, *84*, 205.
[6] T. Ueda, D. Honda, T. Shiromoto, N. Metoki, F. Honda, K. Kaneko, Y. Haga, T. D. Matsuda, T. Takeuchi, A. Thamizhavel, K. Sugiyama, K. Kindo, R. Settai, Y. Ōnuki, *J. Phys. Soc. Jpn*. **2005**, *74*, 2836.
[7] W. Hermes, R.-D. Hoffmann, M. H. Möller, E. Gaudin, B. Chevalier, R. Pöttgen, unpublished results.
[8] B. Chevalier, R. Decourt, B. Heying, F. M. Schappacher, U. Ch. Rodewald, R.-D. Hoffmann, R. Pöttgen, R. Eger, A. Simon, *Chem. Mater*. **2007**, *19*, 28.
[9] B. Chevalier, B. Heying, U. Ch. Rodewald, C. P. Sebastian, E. Bauer, R. Pöttgen, *Chem. Mater*. **2007**, *19*, 3052.
[10] J.-L. Bobet, M. Pasturel, B. Chevalier, *Intermetallics* **2006**, *14*, 544.
[11] B. Chevalier, A. Wattiaux, J.-L. Bobet, *J. Phys.: Condens. Matter* **2006**, *18*, 1743.
[12] R. Pöttgen, Th. Gulden, A. Simon, *GIT-Laborfachzeitschrift* **1999**, *43*, 133.
[13] K. Yvon, W. Jeitschko, E. Parthé, *J. Appl. Crystallogr*. **1977**, *10*, 73.
[14] J.-L. Bobet, S. Pechev, B. Chevalier, B. Darriet, *J. Alloys Compd*. **1998**, *267*, 136.
[15] P. Dordor, E. Marquestaut, G. Villeneuve, *Rev. Phys. Appl*. **1980**, *15*, 1607.
[16] W. Kohn, L. J. Sham, *Phys. Rev. A* **1965**, *140*, 1133.
[17] P. Hohenberg, W. Kohn, *Phys. Rev. B* **1964**, *136*, 864.
[18] A. R. Williams, J. Kübler, C. D. Gelatt, Jr., *Phys. Rev. B* **1979**, *19*, 6094.
[19] V. Eyert, *Int. J. Quantum Chem*. **2000**, *77*, 1007.
[20] V. Eyert, *The Augmented Spherical Wave Method – A. Comprehensive Treatment*, Lect. Notes Phys. 719, Springer, Berlin, Heidelberg **2007**.
[21] S. H. Vosko, L. Wilk, M. Nusair, *Can. J. Phys*. **1980**, *58*, 1200.
[22] G. Bester, M. Fähnle, *J. Phys. Condens. Matter* **2001**, *13*, 11541.
[23] R. Hoffmann, *Angew. Chem*. **1987**, *99*, 871; *Angew. Chem. Int. Ed. Engl*. **1987**, *26*, 846.
[24] R. Dronskowski, P. E. Blöchl, *J. Phys. Chem*. **1993**, *97*, 8617.
[25] B. Chevalier, M. Pasturel, J.-L. Bobet, F. Weill, R. Decourt, J. Etourneau, *J. Solid State Chem*. **2004**, *177*, 752.
[26] B. Chevalier, J.-L. Bobet, M. Pasturel, E. Bauer, F. Weill, R. Decourt, J. Etourneau, *Chem. Mater*. **2003**, *15*, 2181.
[27] J. M. Lawrence, P. S. Riseborough, R. D. Parks, *Rep. Prog. Phys*. **1981**, *44*, 1.
[28] E. D. Mun, Y. S. Kwon, M. H. Jung, *Phys. Rev. B* **2003**, *67*, 033103.
[29] J. P. Kuang, H. J. Cui, J. Y. Li, F. M. Yang, H. Nakotte, E. Brûck, F. R. De Boer, *J. Magn. Magn. Mater*. **1992**, *104 – 107*, 1475.
[30] B. Chevalier, J. Etourneau, *J. Magn. Magn. Mater*. **1999**, *196 – 197*, 880.
[31] W. H. Lee, H. C. Ku, R. N. Shelton, *Phys. Rev. B* **1987**, *36*, 5739.
[32] G. Knebel, M. Brando, J. Hemberger, M. Nicklas, W. Trinkl, A. Loidl, *Phys. Rev. B* **1999**, *59*, 12390.
[33] D. Jaccard, J. Sierro in *Valence Instabilities*, (Eds.: P. Wachter, H. Boppart), North-Holland, Amsterdam **1982**, pp. 409.
[34] J. Sakurai, D. Huo, D. Kato, T. Kuwai, Y. Isikawa, K. Mori, *Physica B* **2000**, *281 – 282*, 98.
[35] M. Houshiar, D. T. Adroja, B. D. Rainford, *Physica B* **1996**, *223 – 224*, 268.
[36] V. Zlatic, I. Milat, B. Coqblin, G. Czycholl, *Physica B* **2002**, *312 – 313*, 171.
[37] V. Zlatic, B. Horvatic, I. Milat, B. Coqblin, G. Czycholl, C. Grenzebach, *Phys. Rev. B* **2003**, *68*, 104432.
[38] B. Cornut, B. Coqblin, *Phys. Rev. B* **1972**, *5*, 4541.
[39] P. Link, D. Jaccard, P. Lejay, *Physica B* **1996**, *225*, 207.